Smart Structures and Systems, *Vol. 31, No. 2 (2023) 155-169*
https://doi.org/10.12989/sss.2023.31.2.155

Extraction of quasi-static component from vehicle-induced dynamic response using improved variational mode decomposition

Zhiwei Chen [1,2], Long Zhao [1], Yigui Zhou [1], Wen-Yu He*[3,4] and Wei-Xin Ren [5]

[1] *Department of Civil Engineering, Xiamen University, Xiamen, 361005, China*
[2] *Fujian Key Laboratory of Digital Simulations for Coastal Civil Engineering, Xiamen, 361005, China*
[3] *Department of Civil Engineering, Hefei University of Technology, Hefei, Anhui 230009, China*
[4] *Anhui Engineering Laboratory for Infrastructural Safety Inspection and Monitoring, Hefei University of Technology, Hefei, Anhui 230009, China*
[5] *College of Civil and Transportation Engineering, Shenzhen University, Shenzhen, Guangdong 518061, China*

(*Received May 30, 2022, Revised September 26, 2022, Accepted November 7, 2022*)

Abstract. The quasi-static component of the moving vehicle-induced dynamic response is promising in damage detection as it is sensitive to bridge damage but insensitive to environmental changes. However, accurate extraction of quasi-static component from the dynamic response is challenging especially when the vehicle velocity is high. This paper proposes an adaptive quasi-static component extraction method based on the modified variational mode decomposition (VMD) algorithm. Firstly the analytical solutions of the frequency components caused by road surface roughness, high-frequency dynamic components controlled by bridge natural frequency and quasi-static components in the vehicle-induced bridge response are derived. Then a modified VMD algorithm based on particle swarm algorithm (PSO) and mutual information entropy (MIE) criterion is proposed to adaptively extract the quasi-static components from the vehicle-induced bridge dynamic response. Numerical simulations and real bridge tests are conducted to demonstrate the feasibility of the proposed extraction method. The results indicate that the improved VMD algorithm could extract the quasi-static component of the vehicle-induced bridge dynamic response with high accuracy in the presence of the road surface roughness and measurement noise.

Keywords: adaptive extraction; dynamic response; moving load; quasi-static components

1. Introduction

A large number of bridges have been built in the world today, with 878,300 highway bridges in China alone by the end of 2019. During the operation period, the accumulation of bridge damage and the decay of resistance develop faster than expected due to vehicle overload and factors such as structural fatigue and material corrosion, which lay a huge safety hazard for the normal operation of bridges (Li *et al*. 2006). Early detection of bridge damage through advanced methods is expected to be an effective way to ensure operation safety. Such methods constructed indicators through the structural properties before and after the damage (Liu *et al*. 2020, Yu *et al*. 2015, Niu *et al*. 2015, Kunwar *et al*. 2013, Roveri and Carcaterra 2012, He and Zhou 2019, Kourehli 2016). Among them, vibration-based damage detection methods (e.g., based on modal frequencies (Narkis 1994), mode shapes (Jaishi and Ren 2006) and their derivatives (Jie and Zhao 2006)) have been normally used in previous studies. However, structural dynamic properties (e.g., frequency) are insensitive to local damage or overly sensitive to changes in environmental factors (e.g., temperature). Besides, accurate measurement of certain structural characteristic indices (e.g., mode shape) requires the cooperation of a large number of sensors. Compared with the above mentioned methods, the vehicle-induced bridge dynamic response based damage detection possesses the following advantages: (1) when the moving load approaches the damage position, the bridge response signal has larger amplitude, and the signal-to-noise ratio is higher (Jie and Zhao 2006); (2) fewer sensors are required during the detection process (Link and Weiland 2009). The vehicle-induced bridge dynamic responses were composed of quasi-static components and dynamic components (Cheng *et al*. 2012, Sun *et al*. 2016, Kim and Kawatani 2008, González and Hester 2013, Hester and González 2017), and the former was found to be more suitable for damage detection (He *et al*. 2017).

Though the quasi-static component response is promising in the field of damage detection, how to accurately extract it from the vehicle-induced bridge dynamic response is challenging. Wang *et al*. (2011) obtained the quasi-static response of a bridge through the action of a slowly moving vehicle to reduce the effect of vehicle-bridge interaction. Zhu and Law (2006) extracted bridge quasi-static components by wavelet transform for vehicle-induced bridge displacement response. Chen *et al*. (2020) extracted quasi-static signals from dynamic strain signals in real bridges based on the analytical mode decomposition (AMD). However, manual intervention is required during the extracting process for the wavelet

*Corresponding author, Ph.D., Professor,
E-mail: wyhe@hfut.edu.cn

ISSN: 1738-1584 (Print), 1738-1991 (Online)

transform and AMD based methods. On the contrary, empirical mode decomposition EMD (Tsakalozos *et al*. 2012) is a recursive method for analyzing non-linear and non-smooth signals in which the signal is adaptively decomposed into oscillatory components (named as intrinsic mode function (IMF)) based on the intrinsic properties of the signal without manual intervention. Taking advantage of this property, Meredith *et al*. (2012) employed the EMD and sliding average filtering to extract the quasi-static components from the vehicle-induced bridge dynamic response.

Studies indicated that the low-frequency quasi-static components and the high-frequency vibration components in the bridge response gradually form mode mixing as the increase of the vehicle velocity and road surface roughness (Roveri and Carcaterra 2012), which would result difficulty in the extraction process. Thus, the extraction process must be full-automatic and effective for response signal with closely-space modes. However, several existing signal processing methods are inadequate to achieve this objective. For example, (1) the low-pass filtering method is less effective in decomposing signal with closely-space modes; (2) the selection of suitable mother wavelet in wavelet transform requires rich experience (Hester and González 2012); (3) the cutoff frequency needs to be set manually when AMD is employed; (4) although the EMD does not require manual intervention, it is less effective for the decomposition of signal with closely-space modes (Rilling and Flandrin 2007).

In this paper, a method for extracting the quasi-static component from vehicle-induced dynamic response using improved variational mode decomposition (VMD) is proposed. The rest of this paper is organized as follows. In Section 2, the relationship between the quasi-static components of the dynamic response and the high-frequency components controlled by the bridge natural frequency and road surface roughness is investigated based on the analytical solution of the vehicle -induced bridge dynamic response. In Section 3, the main challenge of extracting quasi-static components is confirmed. In Section 4, an improved VMD algorithm based on particle swarm optimization (PSO) algorithm and mutual information entropy (MIE) criterion is proposed to achieve the adaptive extraction of quasi-static components from the vehicle -induced bridge dynamic response. In Section 5 and Section 6, numerical examples and real bridge tests are carried out to verify the accuracy, robustness, and applicability of the proposed method. Conclusions of the research are presented in Section 7.

2. Vehicle-induced bridge dynamic response

2.1 Simulation of road roughness

Road roughness is the main excitation source causing vehicle vibration, and affects the safety and smooth comfort of vehicle in operation (Li *et al*. 2020). In this paper, the road roughness is simulated using the power spectral density (PSD) (Morelli *et al*. 1974) recommended by the International Organization for Standardization. The road roughness displacement PSD function ($S_d(f)$) is

$$S_d(f) = S_d(f_0) \cdot (f/f_0)^{-\alpha} \tag{1}$$

where f is the spatial frequency per unit length; $\alpha$is the power spectral density index; f_0 $(= 0.1\ m^{-1})$ is the reference spatial frequency; $S_d(f_0)$ is the displacement PSD function value.

The superposition of sinusoidal functions with different spatial frequencies is employed to simulate the road roughness $y(x)$, i.e.

$$y(x) = \sum_{p=1}^{N} \sqrt{4S_d(f_p)\Delta f}\, cos\left(2\pi f_p x + \theta_p\right) \tag{2}$$

where $f_p = p\Delta f$ is the spatial frequency, $\Delta f = \frac{1}{N\Delta}$, Δ is the load shift step; N is the number of sampling points; θ_p is the random phase angle $(\theta_p \in (0,2\pi))$ which obeys normal random distribution. Noting that $x = vt$ and $\Omega_p = 2\pi f_p v$, thus Eq. (2) can be rewritten as

$$y(t) = \sum_{p=1}^{N} Y_p\, cos\left(\Omega_p t + \theta_p\right) \tag{3}$$

where Y_p is the amplitude of the road roughness.

2.2 Bridge response induced by moving vehicle

As shown in Fig. 1, a single-degree-of-freedom vehicle is assumed to pass over a simply supported bridge at a uniform velocity v, where the contact point between the wheel and the bridge keeps in contact.

The moving vehicle force F is composed of a constant force (F_s) represented by the vehicle's self-weight and an excitation force (F_d) caused by the road roughness.

$$F = F_s + F_d = M_v g + k_v \cdot \sum_{p=1}^{N} Y_p\, cos\left(\Omega_p t + \theta_p\right) \tag{4}$$

where M_v is the vehicle weight; g is the gravitational acceleration; k_v is the vehicle stiffness.

The bridge displacement response induced by moving vehicle can be regarded as the sum of the displacement components caused by the constant force and the simple harmonic force with different frequencies, respectively.

(1) Displacement component caused by the constant force

Suppose the vertical load F_s moves with the velocity

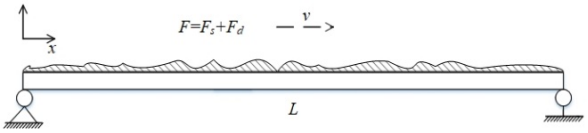

Fig. 1 Vehicle model

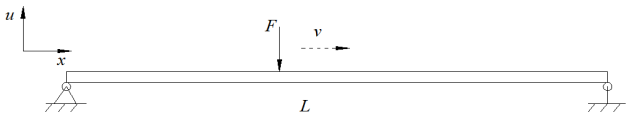

Fig. 2 Simply supported bridge subjected to a moving load

v on a simply supported bridge without considering the damping effect (Fig. 2), the load-displacement differential equation of the bridge can be established as follows

$$\rho A\frac{\partial^2 u(x,t)}{\partial t^2}+\frac{\partial^2}{\partial x^2}[EI\frac{\partial^2 u(x,t)}{\partial x^2}]=F_s\delta(x-vt) \tag{5}$$

where $u(x,t)$ is the displacement response of the bridge, x and t are the location and time of the response; E and I are the modulus of elasticity and moment of inertia; L is the span length; ρ is the mass density of the bridge; A is the cross-sectional area; $\delta(x)$ is the Dirac function.

By assuming the initial displacement and velocity of the bridge are zeros, Yang and Lin (2005) derived the analytical solution for Eq. (5) based on the modal superposition method. The analytical solution of the total displacement response induced by the movin1

g load (u_s) can be decomposed into the moving load frequency component (u_l) with low frequency and the bridge natural frequency component (u_h) with high frequency.

$$u_s=u_l+u_h \tag{6}$$

The low-frequency component u_l controlled by the moving-frequency $\frac{i\pi v}{L}$ is

$$u_l=\frac{2L^3F_s}{\pi^4EI}\sum_{i=1}^{N}\frac{1}{i^4(1-S_i{}^2)}sin\,\omega_v\,t\,sin\frac{i\pi x}{L} \tag{7}$$

where $\omega_v=\frac{i\pi v}{L}$, and S_i is a dimensionless velocity parameter defined as

$$S_i=\frac{i\pi v}{L\omega_n} \tag{8}$$

The high-frequency component u_h controlled by the bridge natural frequency is

$$u_h=-\frac{2L^3F_s}{\pi^4EI}\sum_{i=1}^{N}\frac{S_i}{i^4(1-S_i{}^2)}sin\,\omega_i\,t\,sin\frac{i\pi x}{L} \tag{9}$$

where ω_i is the i^{th} natural frequency of the beam.

According to Eqs. (6)-(8), the amplitudes of the components u_l and u_h decrease i^4 exponentially with the mode order. Therefore, only the contributions of the first *N* orders are need to be considered in Eq. (6).

(2) Displacement component caused by the simple harmonic excitation force.

The load-displacement differential equation of the bridge subjected to the excitation force (F_d) caused by the road roughness can be established as

$$\rho A\frac{\partial^2 u(x,t)}{\partial t^2}+\frac{\partial^2}{\partial x^2}[EI\frac{\partial^2 u(x,t)}{\partial x^2}]=F_d\delta(x-vt) \tag{10}$$

The bridge displacement subjected to simple harmonic excitation can be obtained by using the modal superposition method as

$$\begin{aligned}u_d(x,t)=&\frac{2F_1}{pAL}\sum_{i=1}^{N}\left\{\frac{1}{1-(\lambda_l-S_i)^2}\{sin[(\Omega_p-\omega_v)t+\theta_p]-sin\omega_l t\}\right\}sin\frac{i\pi x}{L}\\&\frac{2F_1}{pAL}\sum_{i=1}^{N}\left\{\frac{1}{1-(\lambda_l+S_i)^2}\{sin[(\Omega_p+\omega_v)t+\theta_p]-sin\omega_l t\}\right\}sin\frac{i\pi x}{L}\end{aligned} \tag{11a}$$

where

$$F_1=k_vY_p \tag{11b}$$

$$\lambda_i=\Omega_p/\omega_i \tag{11c}$$

The response in Eq. (11) can be decomposed into two frequency components as

$$u_d=u_{d1}+u_{d2} \tag{12}$$

The frequency component u_{d1} controlled by $\Omega_n-\omega_v$ is

$$u_{d1}=\frac{2F_1}{mL}\sum_{i=1}^{N}\left\{\frac{1}{1-(\lambda_i-S_i)^2}\{sin[(\Omega_p-\omega_v)t+\theta_p]-sin\,\omega_i\,t\}\right\}sin\frac{i\pi x}{L} \tag{13}$$

The frequency component u_{d2} controlled by $\Omega_n+\omega_v$ is

$$u_2=\frac{2F_1}{mL}\sum_{i=1}^{N}\left\{-\frac{1}{1-(\lambda_i+S_i)^2}\{sin[(\Omega_p+\omega_v)t+\theta_p]-sin\,\omega_i\,t\}\right\}sin\frac{i\pi x}{L} \tag{14}$$

The following conclusions can be drown from Eq. (12): (1) The response of the simply supported bridge is the superposition of the forced vibration with frequencies of $\Omega_p+\omega_v$ and $\Omega_p-\omega_v$ caused by the road roughness; (2) the vibration amplitude of the dynamic component is proportional to the square root of the road roughness coefficient, i.e., the lower the pavement grade, the greater the dynamic component amplitude.

Combining the Eq. (6) and Eq. (12), the bridge displacement response can be rewritten as

$$\begin{aligned}&u(x,t)=u_s(x,t)+u_d(x,t)\\&=\frac{2L^3F_s}{\pi^4EI}\sum_{i=1}^{N}\frac{sin\frac{i\pi x}{l}}{i^4(1-S_i{}^2)}\{sin\,\omega_v\,t-S_o\,sin\,\omega_i\,t\}\end{aligned} \tag{15}$$

$$+\frac{2F_1}{p}\sum_{i=1}^{N}\left\{\frac{1}{1-(\lambda_i-S_i)^2}\{sin[(\Omega_p-\omega_v)t+\theta_p]-\sin\omega_i t\}\right\}sin\frac{i\pi x}{L}$$
$$-\frac{2F_1}{p}\sum_{i=1}^{N}\left\{\frac{1}{1-(\lambda_i+S_i)^2}\{sin[(\Omega_p+\omega_v)t+\theta_p]-\sin\omega_i t\}\right\}sin\frac{i\pi x}{L} \quad (15)$$

It is assumed that $\Omega_p >> \omega_v$ for the highway bridges. Thus, the bridge response can be expressed as a combination of three types of response components with different frequencies. The quasi-static component is controlled by frequency ω_v, the high frequency component is controlled by the bridge natural frequency ω_n, and the remainder component is controlled by vibration frequency Ω_p caused by the road roughness.

When the velocity is close to zero, the moving load can be approximated as a quasi-static load. Then Eq. (15) can be used to derive the analytical solution of the quasi-static u_{st} component of the dynamic response considering the influence of road roughness as

$$u_{st}=u_0\sum_{i=1}^{N}\frac{1}{i^4}sin\,\omega_v\,t\,sin\frac{i\pi\bar{x}}{L} \quad (16)$$

where $\bar{x}=vt$ denotes the location of the load. As the time t for the vehicle passing the bridge changes with the vehicle velocity v, the product of the vehicle velocity v and the time t remains the same, thus the quasi-static component is not affected by the vehicle velocity.

3. Challenge in quasi-static component extraction

In this section, the effect of the vehicle velocity on the low-frequency and high-frequency components of the vehicle-induced bridge response is investigated via numerical examples, and the main challenge of extracting the quasi-static components is confirmed.

The parameters of the bridge are shown in Table 1. The parameters of the three-parameter vehicle model are as follows: mass$m_v=4.0\times10^3$ kg, spring stiffness $k_v=6.0\times10^5\,N/m$, and damping $c_v=1.0\times10^3\,Ns/m$. The road roughness displacement PSD function is set to be $\sqrt{64}\times10^{-6}$ m^3 for B-grade pavement. The measurement point is located in the middle of the span ($x=L/2$). Then the bridge responses induced by the vehicle with different velocities (5 m/s and 20 m/s) are calculated via Eq. (15). Fig. 3 shows the different components (the total displacement response u, bridge natural frequency component u_d, moving load frequency component u_{sh}, and quasi-static component u_{st}) of the bridge displacement response corresponding to a load velocity of 5 m/s. The displacement curve of the simply supported bridge subjected to the moving load is a superposition of three sinusoidal curves. The quasi-static component u_{st} is a sinusoidal half-wave curve and similar to constant force induced response. It is the main trend term of the response controlled by moving-frequency ω_v.

Table 1 The main parameters of the bridge

Parameter	Value
Span length (L)	20 m
Elasticity modulus (E)	2.75×10^{10} N/m^2
Moment of inertia (I)	0.12 m^4
Density (ρ)	1200 kg/m^3
Cross-sectional of area (A)	2.0 m^2

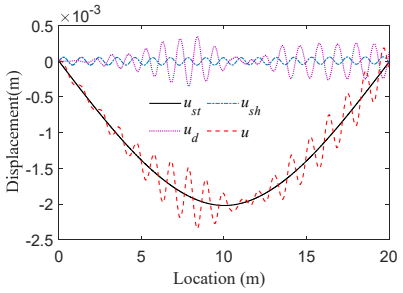

Fig. 3 Different components of the bridge dynamic response (5 m/s)

In order to explore the relationship between the bridge response components and of the vehicle velocity, the spectrogram of the responses when the vehicle velocity is $v=5$ m/s and $v=20$ m/s is presented in Fig. 4. Arrows ω_v, ω_1, and Ω_p denote the frequency of the vehicle, the first natural frequency of the bridge, and the high-frequency component, respectively. The blue dashed lines are the frequency demarcation lines to make the different frequency components more clearly. It can be seen that under the excitation of road roughness, the high-frequency component (Ω_p) controlled by a series of spatial frequencies of the road roughness power spectrum contains rich frequency components; the bandwidth occupied by the moving load frequency component (ω_v) is positively correlated with the vehicle velocity, while the frequency magnitude of the bridge natural frequency component (ω_i) is independent of the vehicle velocity, but the amplitude of the spectrum is positively correlated with the vehicle velocity.

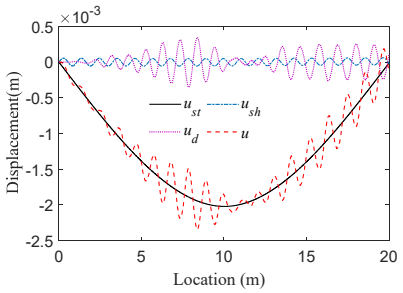

Fig. 4 The amplitudes and frequency of the different response components

As the velocity increases, the bandwidth occupied by the moving load frequency component gradually increases, and the moving load frequency component and the bridge natural frequency component gradually become closely-space modes. For the closely-space modes, the common low-pass filters (such as Butterworth low-pass filter and Gaussian low-pass filter) are insufficient to extract the quasi-static component form the total response.

4. Quasi-static component extraction based on improved VMD algorithm

As stated in the previous section, the vehicle-induced bridge dynamic response consists of a low-frequency quasi-static component and a high-frequency dynamic component, both of which are linear combinations of different frequency sinusoidal functions. As the velocity increases, the bandwidth occupied by the quasi-static components in the frequency domain gradually increases while the position of the bridge natural frequency components remains unchanged. Thus, when the velocity increases to a certain value, the quasi-static components and the bridge natural frequency components gradually approach to become closely-space modes. The decomposition capability of EMD for signals with closely-space modes is insufficient (Zosso and Dragomiretskiy 2014), which leads to modal overlapping and distortion of the decomposed signal. This section aims to propose a quasi-static component extraction method based on the improved VMD algorithm.

4.1 Introduction of the VMD algorithm

VMD is an adaptive signal processing tool developed based on EMD, which uses Wiener filter and Hilbert transform to construct a variational problem for an input signal f (Zosso and Dragomiretskiy 2014). The center frequency and bandwidth of each intrinsic mode component are determined by iteratively searching for the optimal solution of the variational model to achieve effective separation of the signal from low to high frequencies. This variational problem is solved using the alternating direction method of multipliers algorithm (Boyd *et al*. 2010). The specific implementation processes are as follows

(1) Initializing parameters ($\{u_k^1\}$, $\{w_k^1\}$, λ^1, and $n = 0$).
(2) Updating u_k and ω_k according to Eqs. (17)-(18). Where, $u_k(\omega)$ is a frequency domain signal, converted from a time domain signal, according to Parseval/Plancherel's theorem. The value of $u_k^{n+1}(\omega)$ is updated to

$$\hat{u}_k^{n+1}(\omega) = \frac{\hat{f}(\omega) - \sum_{i<k}\hat{u}_i^{n+1}(\omega) + \sum_{i>k}\hat{u}_i^{n+1}(\omega) + (\hat{\lambda}(\omega)/2)}{1 + 2\alpha(\omega - \omega_k^n)^2} \quad (17)$$

where α is the penalty parameter and $f(\omega)$ is a frequency domain signal converted from a time domain signal.
Likewise, the center frequency of each mode component ω_k is the conversion from a time signal to a frequency domain signal, whose value is updated to

$$\omega_k^{n+1} = \frac{\int_0^\infty \omega\,|\hat{u}_k^{n+1}(\omega)|^2 d_\omega}{\int_0^\infty |\hat{u}_k^{n+1}(\omega)|^2\, d_\omega} \quad (18)$$

(3) Updating Lagrange multiplier λ by Eq. (19), the value of $\lambda^{n+1}(\omega)$ is updated to

$$\hat{\lambda}^{n+1}(\omega) = \hat{\lambda}^n(\omega) + \tau\left(\hat{f}(\omega) - \sum_k \hat{u}_k^{n+1}(\omega)\right) \quad (19)$$

In the formula, τ represents the noise tolerance parameter.
(4) Repeating Steps (2)-(3). If $\sum_k \|\hat{u}_k^{n+1} - \hat{u}_k^n\|_2^2 / \|\hat{u}_k^n\|_2^2 < \varepsilon$ or $n = N$, then ending the whole circulation and obtaining k narrowband IMF components.ε is the given discriminant accuracy.

Compared with normally used EMD, VMD possessed the following advantages:

(1) The decomposition mode of VMD has a solid theoretical foundation, and the decomposition results are stable without modal mixing effect as in the EMD (Isham *et al*. 2018).
(2) VMD is essentially composed of a series of Wiener filter groups with strong refinement ability for time-frequency signals. VMD can successfully separate two pure harmonic signals with similar frequencies, and the separated signals are extremely similar to the original signal waveform in the aspect of frequency and other parameters (Fu *et al*. 2018).

However, there are two major problems when applying VMD to extract low-frequency quasi-static component, specific as:

(1) Parameter selection: the number of decomposed IMF components needs to be predetermined when processing signals by the VMD algorithm. The penalty parameter α in the VMD algorithm has a significant impact on the decomposition results. Due to the complexity and variability of the bridge response signal, the selection of the appropriate combination of K and α is a key issue for extracting the low frequency quasi-static signal by the VMD algorithm (Wang *et al*. 2015).
(2) Boundary effect: the signal truncation and Hilbert transform both produce boundary effects, which affects the analysis accuracy. Especially for signals with a high level frequency band overlapping, the VMD algorithm suffer from severe modal mixing and boundary effects, which will lead to decomposition failure (Liu *et al*. 2016).

In view of this, this study proposes an adaptive parameter selection strategy for VMD algorithm based on PSO and an improvement strategy to reduce boundary effect based on MIE criterion.

4.2 Adaptive selection of VMD parameters based on PSO algorithm

In this section, the PSO algorithm with good global search capability is used to optimize the two parameters of the VMD algorithm in parallel automatically, thus avoiding the intervention of subjective factors. The PSO algorithm uses the interactions between individuals in a swarm of particles to find the optimal region of a complex search space (Clerc and Kennedy 2002), and its solution processes are summarized as follows.

Supposing in a D -dimensional space, the population of M particles is $X = (X_1, X_2, \cdots, X_M)$. The position in the D -dimensional search space, velocity, and individual local extremum of the i^{th} particle are $X_i = (x_{i1}, x_{i2}, \cdots, x_{iD})$, $V_i = (v_{i1}, v_{i2}, \cdots, v_{iD})$, and $P_i = (p_{i1}, p_{i2}, \cdots, p_{iD})$, respectively. The population global extreme is $G_i = (g_{i1}, g_{i2}, \cdots, g_{iD})$, and each particle updates its velocity and position by iterating through the individual local extremum and the population global extremum, expressed as in Eq. (20) (Kennedy *et al*. 2001).

$$\left.\begin{array}{c} v_{id}^{k+1} = \omega v_{id}^{k} + c_1\eta\left(p_{id}^{k} - x_{id}^{k}\right) + c_2\eta\left(g_{d}^{k} - x_{id}^{k}\right) \\ x_{id}^{k+1} = x_{id}^{k} + v_{id}^{k+1} \end{array}\right\} \quad (20)$$

where ω is the inertia weight; $d = 1,2,\cdots,D$; $i = 1,2,\cdots,M$; k is the number of current iterations; c_1 and c_2 are the acceleration factor; η is a random number between [0,1].

In order to ensure that the quasi-static components can be extracted accurately and adaptively, a fitness objective function should be determined when searching for the influence parameters of the VMD algorithm using the PSO algorithm. The fitness value is calculated and updated each time when the particle updates its position. As discussed in the previous section, the quasi-static component is more concise and similar to the vehicle-induced bridge dynamic response than the high-frequency vibration component in the vehicle-induced bridge dynamic response. The fitness objective function is defined as in Eq. (21).

$$target = \underset{i=1,2,\ldots M}{argmin}(Ed + SampEn) \quad (21)$$

where Ed is the Euclidean distance between the coordinate $x(j)$ of the peak of the j^{th} separated signal and the coordinate y of the peak of the vehicle-induced bridge dynamic response signal, which is used to evaluate the similarity between separated signals and response signal.

$$Ed = \sqrt{\sum (x(j) - y)^2} \quad (22)$$

$SampEn$ is the sample entropy of the i^{th} separated signal, and used to evaluate the complexity of the separated signal.

$$SampEn(m, r, N) = -\ln\left[\frac{D_i^{m+1}(r)}{D_i^{m}(r)}\right] \quad (23)$$

The magnitude of the sample entropy value reflects the uniformity of the probability distribution. The most uncertain probability distribution has the largest entropy value, and the more complex time series corresponds to larger sample entropy (Tuzikov and Sheynin 2002). It can be seen that the sample entropy value is related to the parameters m and r. However, the trend of the sample entropy is not affected by m and r. In general, when m is taken as 1 or 2 and r is taken as 0.1-0.25 SD (SD is the standard deviation of the data series), the calculated sample entropy has more reasonable statistical characteristics (Zweig and Hufnagel 1990).

When the i^{th} particle locates at position X_i (corresponding to $\alpha$and K), the fitness values of all signal components obtained by VMD at this position are calculated accordingly. The smallest one is deemed as the local minimal fitness value (denoted by mintarget), and the corresponding signal component contains rich structural feature information in the group. In order to search for the global best component that contains the most feature-rich information from the bridge displacement signal, the local minimum entropy value is used as the fitness value in the optimization process, and the minimization of the local minimum entropy value is used as the final search goal. The procedures to optimize the VMD coefficients $\alpha$and K are summarized as follows.

(1) Initializing the parameters of the PSO algorithm and determining the fitness function in the optimization search process.
(2) Taking the parameter combination $[\alpha, K]$ as the particle position, generate a certain number of influencing parameter combinations as the initial position of the particle, and initializing the moving velocity of each particle.
(3) Applying VMD on the signal under different particle positions and calculating the corresponding fitness value ($target$) according to Eq. (21).
(4) Comparing the fitness values, and updating individual local extremes and population global extremes.
(5) Updating the velocity and position of the particle using Eq. (20).
(6) Repeating iterations and go to step (3) until the number of iterations reaches the maximum set value, and then outputting the best fitness value and the position of the particle.

It should be noted that improved VMD algorithm automatically selects the best parameters that suitable for extracting the quasi-static components in which the extraction error due to the manual selection $[\alpha, K]$ can be effectively avoided.

4.3 VMD boundary effect improvement based on MIE criterion

The MIE is used to describe the difference in uncertainty between two random variables in the statistical relevance sense. It can be expressed as

$$I(X, Y) = H(Y) - H(Y|X) \quad (24)$$

where $H(Y)$ is the information entropy of the signal Y; $H(Y|X)$ is the conditional entropy of Y when X is known, they can be calculated through the methods in Cover and Thomas (2005). The theorem of data-processing inequality "If $X \to Y \to Z$, then $I(X,Y) \geq I(X,Z)$" in Cover and Thomas (2005) shows the same change trend of MIE and data inequality. Hence, MIE, which has the same role as inequality in this study, increases with the correlation between X and Y (Hausser and Strimmer 2014), thus it can be used to judge the correlation level between sub-waveforms in the original signal. The signal segment with the largest mutual information value to the signal at the boundary is taken out from the original signal as the best matching signal segment based on the MIE. Further it is translated to both ends of the original signal for the signal extension.

The improved VMD algorithm uses the MIE criterion to extend the signal of the vehicle-induced bridge dynamic response, which effectively avoids the signal discontinuity caused by the incoming and outgoing bridges of the vehicle and the spectral leakage caused by Hilbert at the boundaries.

4.4 Extraction procedure

The procedure to extract the quasi-static components from the vehicle-induced bridge dynamic response is provided in Fig. 5, specific as:

Step 1: Obtaining the bridge displacement response induced by the moving vehicle;
Step 2: Extending the signal of the vehicle-induced bridge dynamic response based on the MIE criterion to obtain a continuous and stable signal;
Step 3: Finding the value of the globally minimized objective function using the PSO algorithm and determine the optimal number of modes K_{opt} and penalty parameter α_{opt};
Step 4: Extracting the low-frequency component of the bridge dynamic response through the VMD method.

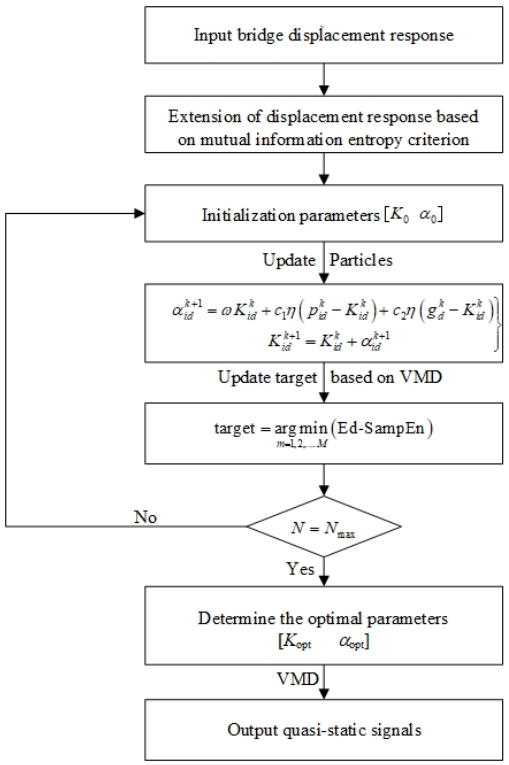

Fig. 5 Flow chart of quasi-static signal extraction

5. Numerical examples

In this section, numerical examples of a simply supported bridge and a two-span continuous girder are used to verify the feasibility of the proposed quasi-static component extraction method in terms of accuracy, robustness and applicability, respectively.

5.1 Accuracy verification

In the previous sections, the moving force model is used instead of the moving vehicle model by assuming that the vehicle mass is much smaller than the bridge mass. However, the vehicle itself is a combined system of rigid body, damping, and spring, and the dynamic characteristics of the vehicle affect the interaction force. In this section, a three-parameter model of mass-spring-damping is used to simulate the moving vehicle (Fig. 6).

The governing equation of the vehicle-bridge system with N finite elements can be expressed as (Li and Au 2014)

$$\begin{Bmatrix} P_b \\ P_v \end{Bmatrix} = \begin{bmatrix} M_b & 0 \\ 0 & M_v \end{bmatrix} \begin{Bmatrix} \ddot{u}_b \\ \ddot{q}_v \end{Bmatrix} + \begin{bmatrix} C_b & C_{bv} \\ C_{vb} & C_v \end{bmatrix} \begin{Bmatrix} \dot{u}_b \\ \dot{q}_v \end{Bmatrix} + \begin{bmatrix} K_b & K_{bv} \\ K_{vb} & K_v \end{bmatrix} \begin{Bmatrix} u_b \\ q_v \end{Bmatrix} \tag{25}$$

where M_b and K_b are the system mass matrix and stiffness matrix of the bridge, respectively; C_b is the damping matrix which can be represented as $C_b = a_1 M_b + a_2 K_b$, a_1 and a_2 are the two parameters in the Rayleigh damping model; $\ddot{u}_b$, $\dot{u}_b$ and u_b are the acceleration, velocity, and displacement response of the bridge, respectively; M_v, C_v and K_v are the mass, damping and stiffness matrix of the vehicle, respectively; $\ddot{q}_v$, $\dot{q}_v$ and q_v are the acceleration, velocity, and displacement response of the vehicle, respectively; P_b and P_v are the external loads.

The main parameters of the bridge are shown in Table 1. The vehicle model is same as in Section 3, and the vehicle velocities are $v = 20$ km/h, $v = 50$ km/h, and $v = 100$ km/h, respectively. The measurement point is located at the middle span, and the sampling frequency is set to be1000 Hz. Fig. 7 shows the measured displacement

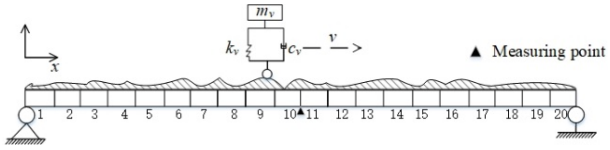

Fig. 6 Vehicle-bridge coupling model

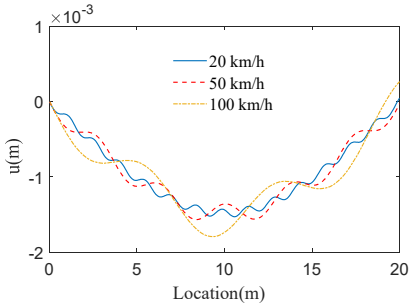

Fig. 7 Vehicle-induced bridge displacement response

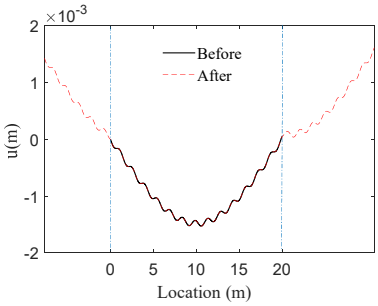

Fig. 8 Bridge displacement response extension

response induced by the vehicle with different moving velocities. It can be seen that the number of vibration periods of the bridge response decreases and the high frequency vibration amplitude increases with the increasing of the vehicle velocity.

The quasi-static components are extracted from the measured responses (Fig. 7) using the improved VMD algorithm described in Section 4.4. Firstly, the bridge responses are extended by the MIE criterion described in Section 4.3, and the corresponding results are plotted in Fig. 8. Secondly, the PSO algorithm is used to find the globally optimal number of modes K and penalty parameter α by iteration (Fig. 9). The population size S of the PSO algorithm and the maximum number of iterations of the population are both set to be 20 (Clerc and Kennedy 2002). The acceleration factors c_1 and c_2 are set to be 1.5 (Clerc and Kennedy 2002). The bridge response induced by the vehicle moving at a very low speed is considered as the theoretical static response. Fig. 9 indicates that the quasi-static component extraction results tend to be stable. The error between the extracted quasi-static component and the theoretical static response decreases with the iteration process, and tends to be zero expect the areas near the supports when the iteration number is 20. Finally, the quasi-static components are extracted via the improved VMD algorithm based on the MIE criterion and the optimal parameters selected by PSO algorithm. The extraction results are presented in Fig. 10. The extracted quasi-static components are well identical with the theoretical static response when the moving velocity is $v = 20$ km/h, which clearly indicates that the proposed method can extract the quasi-static components adaptively and accurately.

The performances of the VMD method, the traditional low-pass filtering represented by Butterworth, AMD, EMD, wavelet transform and single channel blind source separation methods are compared to verify the superiority of the proposed method. The quasi-static extraction results obtained by the above mentioned methods are plotted in Fig. 11. Both AMD and VMD perform well when the velocity is 50 km/h (Fig. 11(a)). However, the mode mixing aggravates when the velocity reaches 100 km/h as the low-frequency quasi-static signal is gradually close to the high-frequency signal (Fig. 11(b)). Compared to the theoretical static components, obvious errors can be founded in the quasi-static components extracted by the traditional low-pass filtering method, AMD, and EMD algorithms (Fig. 11(b)). The selected wavelet scales in the wavelet transform have a great influence on the extraction accuracy (Fig. 11(c)). Desirable results are obtained when Daubechies 10 (db10) is selected while remarkable errors appear when Daubechies 6 (db6), and Daubechies 8 (db8) are selected (Fig. 11(c)). Thus, the difficulty in selection of wavelet scales would hinder the application of wavelet transform in quasi-static components extraction. As the fast moving vehicle-induced dynamic response is measured via a single sensor, only the single-channel based signal processing tools are applicable to fulfill the extraction target. The performance of the single-channel blind source separation algorithm does not comply with the requirements, which may be caused by the fact that the quasi-static components and the high-frequency

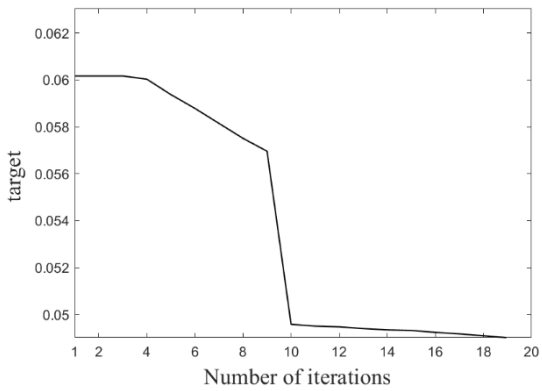

(a) Iterative curves of local adaptation minima

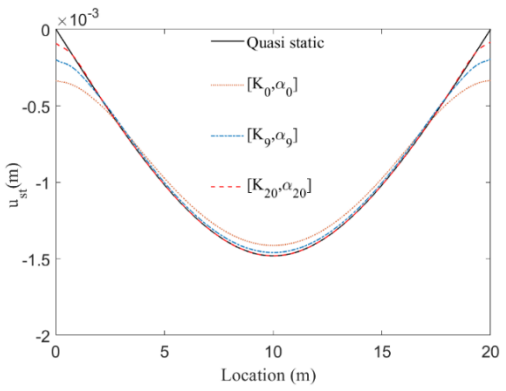

(b) Extraction results with different optimal parameter combination

Fig. 9 PSO iterative process

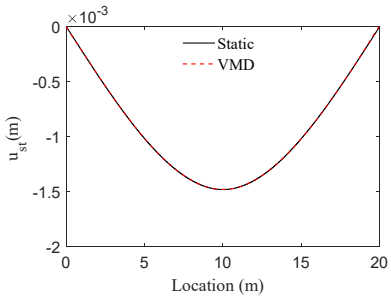

Fig. 10 VMD extracted quasi-static components at vehicle speed of 20 km/h

components of the vehicle-induced dynamic response are not in a mutually independent state (Castiglione *et al*. 2018, Sadhu *et al*. 2017).

In order to quantify the discrepancy between the identified results and theoretical results, three indexes, i.e., relative error of the peak value, relative error of the peak value position, and total relative error are defined for comparison.

$$\delta = \left| \frac{\bar{u}_{l,max} - u_{l,max}}{u_{l,max}} \right| \times 100\% \tag{26}$$

where $\bar{u}_{l,max}$ and $u_{l,max}$ denote the maximum values of the theoretical static response and the extracted quasi-static component, respectively.

The relative error of the peak value position is defined as

$$k = \left| \frac{X(\bar{u}_{l,max}) - X(u_{l,max})}{L} \right| \times 100\% \tag{27}$$

where $X(s_0)$ is the x -coordinate of the data point s_0.

The total relative error is defined as

$$r = \frac{\sum_{i=1}^{N} |\bar{u}_l(i) - u_l(i)|}{\sum_{i=1}^{N} |u_l(i)|} \times 100\% \tag{28}$$

where $\bar{u}_l$ and u_l denote the theoretical static response and the extracted quasi-static component, respectively.

The evaluation indexes calculated according to Eqs. (26)-(28) are listed in Table 2. When the velocity is 20 km/h, the three evaluation indexes δ, k and r are all less than 0.1%, which indicate that the low-frequency quasi-static components extracted by the proposed method are very close to the theoretical solution. However, the three evaluation indexes gradually increase with the increase of the vehicle moving velocity. When the velocity is 100 km/h, the evaluation index r calculated from the quasi-static response and the theoretical static response extracted by the AMD algorithm reaches 6%, and the peak magnitude and position are greater than 3%. However, the error of the quasi-static response extracted by the improved VMD method is less than 3% with respect to the theoretical static response for all three indexes. Compared with AMD, the improved VMD algorithm proposed in this paper can extract the quasi-static components of the vehicle-induced bridge dynamic response more accurately and without manual intervention during the extraction.

5.2 Robustness verification

(1) Road roughness

Road roughness is one of the main excitation sources for the vertical vibration and significantly affects the dynamic

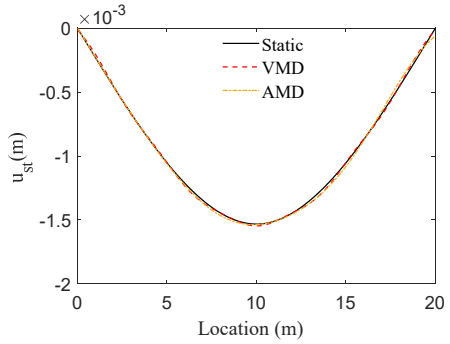

(a) VMD and AMD (50 km/h)

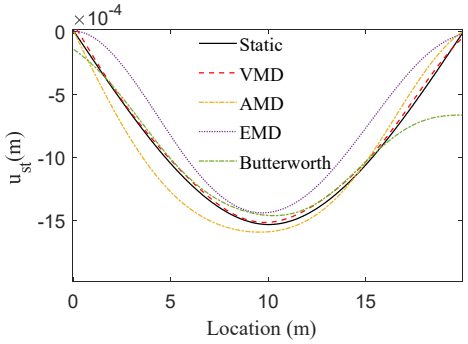

(b) VMD and AMD (100 km/h)

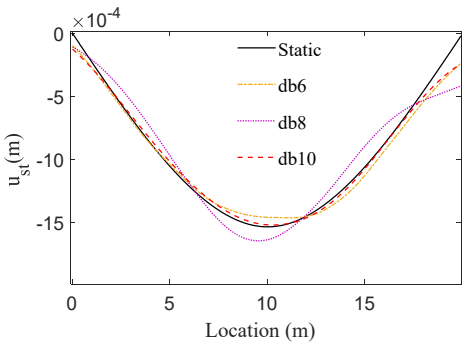

(c) Wavelet Transform method

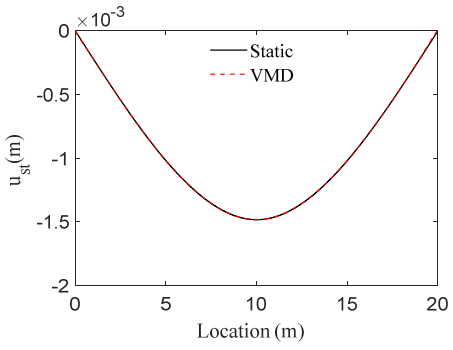

(d) Blind source separation method

Fig. 11 Comparison of quasi-static components and theoretical static components extracted by different method

Table 2 Evaluation indexes under different vehicle speed

Vehicle speed (km/h)	$\bar{u}_{st,max}$ (10^{-3} m)	$u_{st,max}$ (10^{-3} m)	$X(\bar{u}_{st,max})$ (m)	$X(u_{st,max})$ (m)	δ (%)		k (%)		r (%)	
					VMD	AMD	VMD	AMD	VMD	AMD
20	1.532	1.5318	10.00	9.999	0.013	/	0.001	/	0.008	/
50	1.532	1.533	10.00	9.833	0.065	0.56	0.83	2.68	0.61	0.63
100	1.532	1.515	10.00	9.722	1.110	3.95	1.39	4.71	2.51	6.00

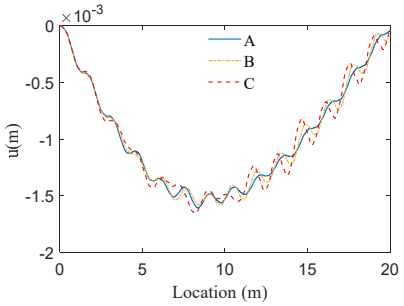

Fig. 12 Bridge displacement response at different road surface roughness

response of bridges. Therefore, this subsection analyzes the effect of road roughness (grade A, B, and C) on the proposed method. The vehicle-bridge model is the same as in the previous sections, and the vehicle velocity is set to be50 km/h. The dynamic responses of the bridge with different road grade are shown in Fig. 12. It can be seen that the magnitude of the bridge response increases with the road grade. Then the optimal parameter combinations are calculated based on the PSO algorithm as $[\alpha_A, K_A] = [5{,}500]$, $[\alpha_B, K_B] = [5{,}1045]$, and $[\alpha_C, K_C] = [8{,}508]$ for the grade A, B, and C road, respectively. The vehicle-induced bridge responses are extended based on the MIE criterion and then processed by the VMD algorithm with the optimal parameter combinations. Fig. 13 provides the extracted low-frequency quasi-static components, and they are found to be in good agreement with the theoretical static response. The corresponding evaluation indexes are calculated according to Eqs. (26)-(28) and summarized in Table 3. The maximum values of δ, k and r are 1.31%, 0.91% and 1.18%, respectively, which demonstrates that the proposed method can accurately extract the quasi-static components with different road roughness.

(2) Measurement noise

In practice, the dynamic response signals are inevitably polluted by measurement noise. The Gaussian white noise with zero mean value is added into the bridge response.

$$u_z = u + E_p N_{noise} \times \sigma(u) \tag{29}$$

Where u_z is the displacement response signal with noise; E_p is the noise level; N_{noise} is a vector of independent random variables following a standard normal distribution, and $\sigma(u)$ is the standard deviation of the bridge displacement response.

The parameters of the vehicle-bridge model, the moving vehicle velocity, and the location of the measurement points are kept the same as in the previous sections. Three noise levels, i.e., 1%, 5%, and 10% are considered separately, and the bridge displacement response with 10% noise is plotted

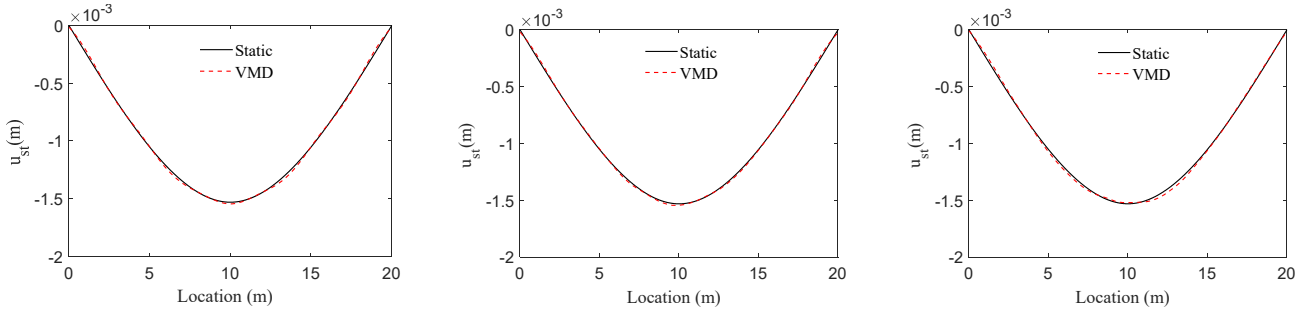

(a) Grade A (b) Grade B (c) Grade C

Fig. 13 VMD extracted quasi-static components with different road surface roughness

Table 3 Evaluation indexes under the different road grade

Road grade	$\bar{u}_{st,max}$ (10^{-3} m)	$u_{st,max}$ (10^{-3} m)	$X(\bar{u}_{st,max})$ (m)	$X(u_{st,max})$ (m)	δ (%)	k (%)	r (%)
A	1.532	1.535	10.00	10.144	0.19	0.72	1.08
B	1.532	1.536	10.00	10.182	0.26	0.91	0.44
C	1.532	1.552	10.00	10.072	1.31	0.36	1.18

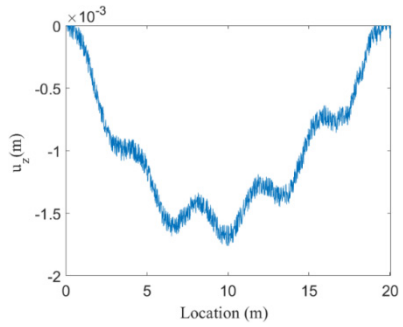

Fig. 14 Bridge responses with 10% noise

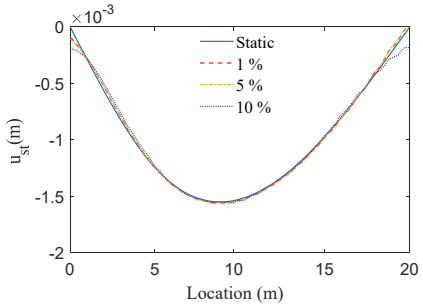

Fig. 15 VMD extracted quasi-static components with different noise level

in Fig. 14. Following the same procedures as in "(1) Road roughness", the low-frequency quasi-static components are extracted and presented in Fig. 15. The extracted results fit well with the theoretical static solution when the noise levels are 1% and 5%. However, vibrations can be found in the quasi-static component when the noise level is 10%. The corresponding evaluation indexes are compared in Table 4. The maximum values of δ, k and r are 0.67%, 1.20% and 2.62%, respectively, which demonstrates that measurement noise doesn't affects the performance of the proposed method too much.

Table 5 The main parameters of the bridge

Parameter	Value
Span length (L)	$L = 20$ m $\times$ 2
Elasticity modulus (E)	2.75×10^{10} N/m^2
Moment of inertia (I)	0.12 m^4
Density (ρ)	2400 kg/m^3
Cross-sectional of area (A)	2.0 m^2

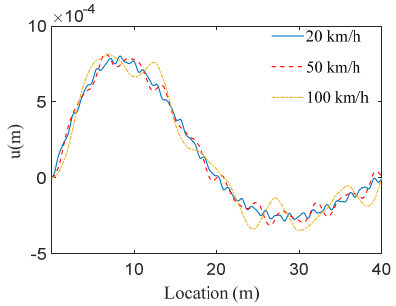

Fig. 17 Displacement response of bridge caused by vehicle with different speed

5.3 Applicability verification

In this subsection, the influence of bridge type on the proposed method is investigated using a two-span continuous bridge. The bridge diagram of the two-span continuous bridge can be seen in Fig. 16, and the parameters are shown in Table 5. The vehicle model is the same as in the previous subsection and the vehicle movement velocity is set to be $v = 20$ km/h, $v = 50$ km/h, and $v = 100$ km/h respectively. Fig. 17 shows the bridge displacement responses caused by the moving vehicle with different velocities. The low-frequency quasi-static components are extracted by the improved VMD algorithm as in Section 5.2 (Fig. 18), and they coincide with the theoretical static solution. Table 6 lists the evaluation indexes calculated by Eqs. (26)-(28). When the velocity is

Table 4 Evaluation indexes under different noise level

Noise level (%)	$\bar{u}_{st,max}$ (10^{-3} m)	$u_{st,max}$ (10^{-3} m)	$X(\bar{u}_{st,max})$ (m)	$X(u_{st,max})$ (m)	δ (%)	k (%)	r (%)
1	1.532	1.5217	10.00	9.95	0.67	0.25	1.56
5	1.532	1.5224	10.00	9.92	0.63	0.40	1.68
10	1.532	1.524	10.00	9.76	0.52	1.20	2.62

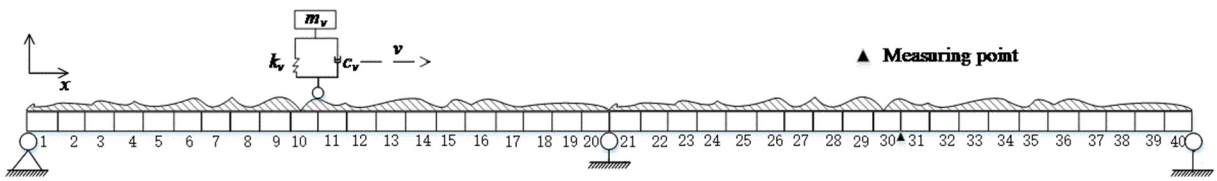

Fig. 16 Vehicle-bridge coupling mod

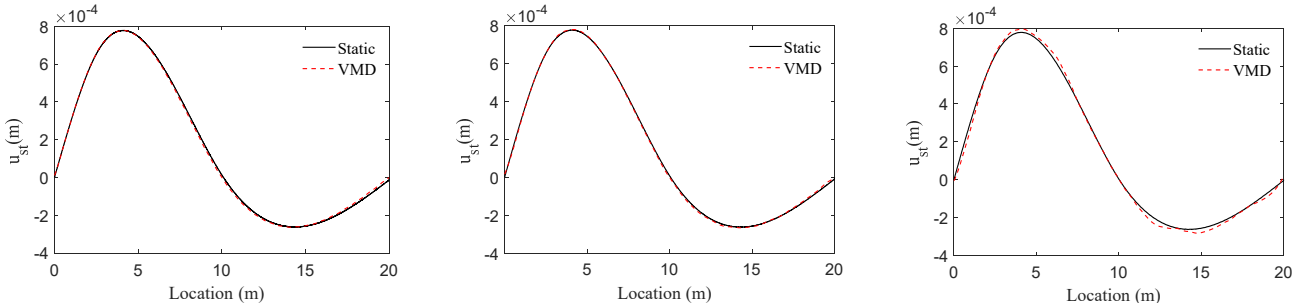

(a) 20 km/h (b) 50 km/h (c) 100 km/h

Fig. 18 VMD extracted quasi-static components with different speed of the continues beam

Table 6 Evaluation indexes of the continuous bridge under different speed

Vehicle speed (km/h)	$\bar{u}_{st,max}$ (10^{-4} m)	$u_{st,max}$ (10^{-4} m)	$X(\bar{u}_{st,max})$ (m)	$X(u_{st,max})$ (m)	δ (%)	k (%)	r (%)
20	7.806	7.818	10.00	10.04	0.15	0.20	0.61
50	7.806	7.831	10.00	10.15	0.32	0.75	1.57
100	7.806	7.980	10.00	10.07	2.23	0.35	4.30

20 km/h, the three evaluation indexes are all less than 1%, which means that the quasi-static components extracted by the proposed method are very close to the theoretical static solution. The three evaluation indexes and the extraction errors of the low-frequency quasi-static components increase with the vehicle velocity. This conclusion is similar as in the simply supported beam.

6. Real bridge applications

The Tongan Line of the Xiamen Bus Rapid Transit System (BRT) starts from Binhai Avenue, and ends at Tongan Junction Station. The selected test bridge is a three-span concrete box girder bridge with a total length of 90 m (Fig. 19). During the normal operation of BRT, strain sensors are placed at 1/4, 1/2 and 3/4 of the main span. The bridge and the corresponding sensor locations (L1, L2 and L3) are shown in Fig. 20. The strain responses of the bridge are measured and stored in the health monitoring system platform. The strain responses measured during the time period of November 2, 20:00-20:30 are selected in this study, and the strain responses at L1 are shown in Fig. 21.

Fig. 19 Elevation of BRT

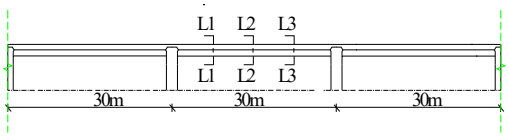

Fig. 20 The arrangement of the strain sensor

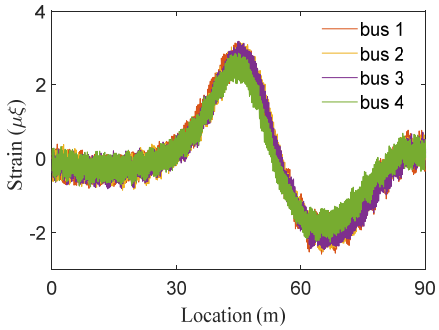

Fig. 21 Measured strain response at the L1 measurement point

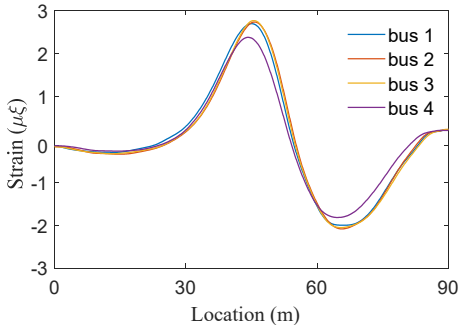

Fig. 22 Quasi-static strain responses of L1 measurement points extracted by the improved VMD

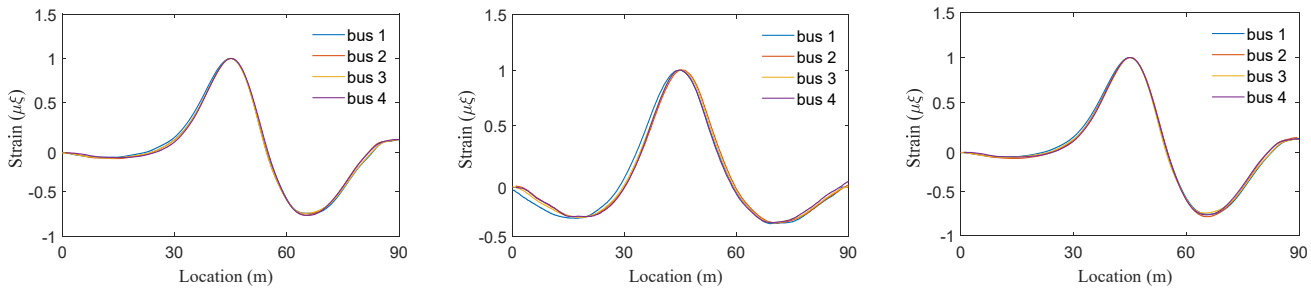

(a) L1 (b) L2 (c) L3

Fig. 23 Extraction results of improved VMD algorithm

During this period, there were 4 vehicles passed through the bridge in the forward direction (Tongan Station - Binhai Station).

It should be noted that the load weights acting on the bridge vary due to the different passenger number of the BRT vehicle, which results in different peak locations and magnitudes in the strain responses at the same location. The improved VMD algorithm is applied on the strain responses (Fig. 21), and the extracted quasi-static components are presented in Fig. 22. The extracted quasi-static strains are smooth in shape for each vehicle, but the maximum strain values vary slightly due to the different number of passengers in each BRT vehicle. In order to avoid the influence of the weight variation caused by the different number of passengers, the measured strain data are normalized to the maximum strain. Then the normalized measured strain responses are used as the input signal to extract the quasi-static components via the improved VMD algorithm, and the results are presented in Fig. 23. The extracted quasi-static components are very close in peak position, peak value and strain shape for each vehicle at different measurement points. The quasi-static components are identified stably for different measurement points even under the adverse effects induced by road roughness and measurement noise, which convincingly verifies the effectiveness of the proposed method.

7. Conclusions

This paper investigated the accurate and adaptive extraction of quasi-static components from the dynamic response of a bridge moving at high velocity. Firstly, the analytical solutions of the frequency components caused by road roughness, high-frequency dynamic components controlled by bridge natural frequency and quasi-static components in the vehicle-induced bridge response were derived. The quasi-static components were found to be independent of the vehicle velocity and road roughness, and could better reflect the inherent characteristics of the bridge. Secondly, the main challenge of extracting the quasi-static components from the vehicle-induced bridge dynamic response was systematically analyzed. The increase of vehicle velocity would cause the high-frequency and low-frequency components of the vehicle-induced bridge dynamic response to gradually approach each other in the frequency domain and form mode mixing, which revealed the reason why the extraction effect of quasi-static components by the common low-pass filtering method decreased as the velocity increased. Then the relationship between the quasi-static components and the vehicle-induced bridge dynamic response was analyzed systematically, and an improved VMD algorithm for adaptively extracting the quasi-static components was proposed based on the PSO algorithm and the MIE criterion. The numerical examples and real bridge tests verified that the improved VMD algorithm could extract the quasi-static component of the vehicle-induced bridge dynamic response with high accuracy considering the road roughness, vehicle dynamic effect, vehicle velocity, measurement noise and different bridge. Compared to the traditional low-pass filtering represented by Butterworth, AMD, EMD, wavelet transform and single channel blind source separation methods, the proposed method had obvious superiority in extracting the quasi-static component.

Credit authorship contribution statement

Zhiwei Chen: Conceptualization, Methodology, Funding acquisition.
Long Zhao: Numerical Analysis, Experiment.
Yigui Zhou: Writing-original draft.
Wen-Yu He: Conceptualization, Writing-review & editing, Funding acquisition.
Wei-Xin Ren: Conceptualization, Funding acquisition.

Declaration of competing interest

The authors declare that they have no known competing financial interests of personal relationships that could have appeared to influence this work reported in this paper.

Acknowledgments

The authors wish to acknowledge the financial supports from the National Natural Science Foundation of China (52278319, 51878234 and 51778204), Natural Science Foundation for Distinguished Young Scholars of Anhui Province (2208085J20), and Shenzhen Science and Technology Program (No. KQTD20180412181337494).

Any opinions and concluding remarks presented in this paper are entirely those of the authors.

References

Boyd, S., Parikh, N., Chu, E., Peleato, B. and Eckstein, J. (2010), "Distributed optimization and statistical learning via the alternating direction method of multipliers", *Found. Trends Mach. Learn.*, **3**, 1-122. https://doi.org/10.1561/2200000016

Castiglione, R., Antoni, J. and Garibaldi, L. (2018), "Separation and identification of structural modes in largely underdetermined scenarios using frequency banding", *J. Sound Vib.*, **414**, 192-217. https://doi.org/10.1016/j.jsv.2017.10.033

Chen, Z., Zhou, Y., He, W.Y. and Liu, M. (2020), "Bridge damage detection using quasi-static component of moving vehicle-induced dynamic response", *Int. J. Computat. Methods*, **18**(06), 2042001. https://doi.org/10.1142/S0219876220420013

Cheng, C.C., Yu, C.P., Ke, Y.T. and Hsu, K.T. (2012), "Evaluation of bridge span by recovered stiffness data obtained with moving vehicle loadings", *Proceedings of Health Monitoring of Structural and Biological Systems 2012*, San Diego, CA, USA, Vol. 8348, pp. 635-641. https://doi.org/10.1117/12.915142

Clerc, M. and Kennedy, J. (2002), "The particle swarm-explosion, stability, and convergence in a multidimensional complex space", *IEEE Transact. Evolut. Computat.*, **20**, 1671-1676. https://doi.org/10.1109/4235.985692

Cover, T. and Thomas, J. (2005), "Data compression", In: *Elements of Information Theory*, (T.M. Cover and J.A. Thomas Eds.). https://doi.org/10.1002/047174882X.ch5

Fu, Z., Zeng, C. and Li, Y. (2018), "A Novel Methodology of Inter-Harmonic Detection Based on VMD", *Proceedings of 2018 10th International Conference on Modelling, Identification and Control* (*ICMIC*), Guiyang, China, July. https://doi.org/10.1109/ICMIC.2018.8529924

González, A. and Hester, D. (2013), "An investigation into the acceleration response of a damaged beam-type structure to a moving force", *J. Sound Vib.*, **332**, 3201-3217. https://doi.org/10.1016/j.jsv.2013.01.024

Hausser, J. and Strimmer, K. (2014), "Estimation of entropy, mutual information and related quantities. R package version 1.2. 1".

He, J. and Zhou, Y. (2019), "A novel mode shape reconstruction method for damage diagnosis of cracked beam", *Mech. Syst. Signal Process.*, **122**, 433-447. https://doi.org/10.1016/j.ymssp.2018.12.045

He, W.Y., Ren, W.X. and Zhu, S. (2017), "Damage detection of beam structures using quasi-static moving load induced displacement response", *Eng. Struct.*, **145**, 70-82. https://doi.org/10.1016/j.engstruct.2017.05.009

Hester, D. and González, A. (2017), "A discussion on the merits and limitations of using drive-by monitoring to detect localised damage in a bridge", *Mech. Syst. Signal Process.*, **90**, 234-253. https://doi.org/10.1016/j.ymssp.2016.12.012

Jie, L.I. and Zhao, X. (2006), "A super-element approach for structural identification in time domain", *Front. Mech. Eng.*, **1**(2), 215-221. https://doi.org/10.1007/s11465-006-0004-4

Kennedy, J., Eberhart, R.C. and Shi, Y. (2001), "Ch. 7: The Particle Swarm", In: *Swarm Intelligence*, pp. 287-325. https://doi.org/10.1016/B978-155860595-4/50007-3

Kim, C.W. and Kawatani, M. (2008), "Pseudo-static approach for damage identification of bridges based on coupling vibration with a moving vehicle", *Struct. Infrastr. Eng.*, **4**, 371-379. https://doi.org/10.1080/15732470701270082

Kunwar, A., Jha, R., Whelan, M. and Janoyan, K. (2013), "Damage detection in an experimental bridge model using Hilbert–Huang transform of transient vibrations", *Struct. Control Health Monitor.*, **20**, 1-15. https://doi.org/10.1002/stc.466

Hester, D. and Gonzalez, A. (2012), "A wavelet-based damage detection algorithm based on bridge acceleration response to a vehicle", *Mech. Syst. Signal Process.*, **28**, 145-166. https://doi.org/10.1016/j.ymssp.2011.06.007

Isham, M.F., Leong, M.S., Meng, H.L. and Ahmad, Z.A. (2018), "Variational mode decomposition for rotating machinery condition monitoring using vibration signals", *Transact. Nanjing Univ. Aeronaut. Astronaut.*, **35**(1), 38-50. https://doi.org/10.16356/j.1005-1120.2018.01.038

Jaishi, B. and Ren, W.X. (2006), "Damage detection by finite element model updating using modal flexibility residual – ScienceDirect", *J. Sound Vib.*, **290**, 369-387. https://doi.org/10.1016/j.jsv.2005.04.006

Kourehli, S.S. (2016), "Structural damage diagnosis using incomplete static responses and LS-SVM", *Inverse Probl. Sci. Eng.*, **25**(3), 418-433. https://doi.org/10.1080/17415977.2016.1169277

Li, Z. and Au, F. (2014), "Damage detection of a continuous bridge from response of a moving vehicle", *Shock Vib.*, **2014**, 1-7. https://doi.org/10.1155/2014/146802

Li, H.J., Ou, J., Zhao, X., Zhou, W., H. Li, Zhou, Z. and Yang, Y. (2006), "Structural health monitoring system for the Shandong Binzhou Yellow River highway bridge", *Comput.-Aided Civil Infrastr. Eng.*, **21**, 306-317. https://doi.org/10.1111/j.1467-8667.2006.00437.x

Li, J., Zhu, X., Law, S.S. and Samali, B. (2020), "Time-varying characteristics of bridges under the passage of vehicles using synchroextracting transform", *Mech. Syst. Signal Process.*, **140**, p. 106727. https://doi.org/10.1016/j.ymssp.2020.106727

Link, M. and Weiland, M. (2009), "Damage identification by multi-model updating in the modal and in the time domain", *Mech. Syst. Signal Process.*, **23**, 1734-1746. https://doi.org/10.1016/j.ymssp.2008.11.009

Liu, S., Tang, G., Wang, X. and He, Y. (2016), "Time-frequency analysis based on improved variational mode decomposition and teager energy operator for rotor system fault diagnosis", *Mathe. Probl. Eng.*, 2016. https://doi.org/10.1155/2016/1713046

Liu, J., Chen, S., Berges, M., Bielak, J. and Noh, H.Y. (2020), "Diagnosis algorithms for indirect structural health monitoring of a bridge model via dimensionality reduction", *Mech. Syst. Signal Process.*, **136**, 106454. https://doi.org/10.1016/j.ymssp.2019.106454

Meredith, J., Gonzalez, A. and Hester, D. (2012), "Empirical mode decomposition of the acceleration response of a prismatic beam subject to a moving load to identify multiple damage locations", *Shock Vib.*, **19**, 845-856. https://doi.org/10.1155/2012/804590

Morelli, C., Gantar, C., Honkasalo, T., Mcconnell, R.K. and Wahlen, C.T. (1974), "The International Organization for Standardization (ISO)", New Political Economy.

Narkis, Y. (1994), "Identification of crack location in vibrating simply supported beams", *J. Sound Vib.*, **172**, 549-558. https://doi.org/10.1006/jsvi.1994.1195

Niu, J., Zong, Z.H. and Chu, F.P. (2015), "Damage identification method of girder bridges based on finite element model updating and modal strain energy", *Sci. China Technol. Sci.*, **58**, 701-711. https://doi.org/10.1007/s11431-014-5763-2

Rilling, G. and Flandrin, P. (2007), "One or two frequencies? The empirical mode decomposition answers", *IEEE Transact. Signal Process.*, **56**, 85-95. https://doi.org/10.1109/TSP.2007.906771

Roveri, N. and Carcaterra, A. (2012), "Damage detection in structures under traveling loads by Hilbert–Huang transform", *Mech. Syst. Signal Process.*, **28**, 128-144. https://doi.org/10.1016/j.ymssp.2011.06.018

Sadhu, A., Narasimhan, S. and Antoni, J. (2017), "A review of

output-only structural mode identification literature employing blind source separation methods", *Mech. Syst. Signal Process.*, **94**, 415-431. https://doi.org/10.1016/j.ymssp.2017.03.001

Sun, Z., Nagayama, T., Su, D. and Fujino, Y. (2016), "A damage detection algorithm utilizing dynamic displacement of bridge under moving vehicle", *Shock Vib.*, **2016**, 8454567. https://doi.org/10.1155/2016/8454567

Tsakalozos, N., Drakakis, K. and Rickard, S. (2012), "A formal study of the nonlinearity and consistency of the Empirical Mode Decomposition", *Signal Process.*, **92**, 1961-1969. https://doi.org/10.1016/j.sigpro.2011.09.014

Tuzikov, A. and Sheynin, S. (2002), "Symmetry measure computation for convex polyhedra", *J. Mathe. Imag. Vis.*, **16**, 41-56. https://doi.org/10.1023/A:1013986402264

Wang, C.Y., Huang, C.K. and Chen, C.S. (2011), "Damage assessment of beam by a quasi-static moving vehicular load", *Adv. Adapt. Data Anal.*, **03**, 417-445. https://doi.org/10.1142/S1793536911000908

Wang, Y., Markert, R., Xiang, J. and Zheng, W. (2015), "Research on variational mode decomposition and its application in detecting rub-impact fault of the rotor system", *Mech. Syst. Signal Process.*, **60**, 243-251. https://doi.org/10.1016/j.ymssp.2015.02.020.

Yang, Y.B. and Lin, C.W. (2005), "Vehicle–bridge interaction dynamics and potential applications", *J. Sound Vib.*, **284**(1-2), 205-226. https://doi.org/10.1016/j.jsv.2004.06.032

Yu, Z., Xia, H., Yin, Y.G. and Sun, D.H. (2015), "Bridge damage identification based on wavelet transform and Lipschitz exponent", *Zhendong yu Chongji/J. Vib. Shock*, **34**, 65-69. https://doi.org/10.13465/j.cnki.jvs.2015.14.012

Zhu, X. and Law, S. (2006), "Wavelet-based crack identification of bridge beam from operational deflection time history", *Int. J. Solids Struct.*, **43**, 2299-2317. https://doi.org/10.1016/j.ijsolstr.2005.07.024

Zosso, D., and Dragomiretskiy, K. (2014), "Variational mode decomposition", *IEEE Transact. Signal Process.*, **62**(3), 531-544. https://doi.org/10.1109/TSP.2013.2288675

Zweig, D. and Hufnagel, R. (1990), "Hilbert transform algorithm for fringe-pattern analysis", In: *Advanced Optical Manufacturing and Testing*, Vol. 1333, pp. 295-302. https://doi.org/ 10.1117/12.22815

BS